

INVESTIGATION OF HELICOPTER AIRFRAME NORMAL MODES

R. W. White
Westland Helicopters Limited
Yeovil, Somerset, England

1. Introduction

The work reported herein is part of a continuing long term programme of government sponsored research into the dynamic characteristics of helicopter airframes.

The objectives of the research were to assess general methods of analysing helicopter vibration, with particular reference to the use of normal modes in the forced response problem.

The normal modes of a Wessex helicopter were isolated (using multi-point excitation), quantified and compared with modes calculated from minimum complexity finite element analysis. Both sets of modes were used to predict forced response and were compared with measured response to rotor head excitation. Acceptable agreement has been achieved between measured and calculated modes and predicted forced response amplitudes were sufficiently close to the measured values to give confidence in both testing techniques and the use of normal modes in the forced response problem.

The research was conducted using the 'total dynamics' concept where one small interdependent team was responsible for the entire project. It was found that the use of such a concept was totally justified. Furthermore it is believed that the use of the techniques reported herein brings a new level of understanding to the airframe dynamics problem.

2. Normal Mode TheoryThe Existence, Excitation and Characteristics of Forced Damped Normal Modes

Initially the theory is developed to show the existence of normal modes in a linear system with proportional hysteretic damping. The equation of motion of a linear structure subjected to a set of harmonic real forces may be written.

$$M\ddot{x}(t) + (K + iH)\dot{x}(t) = fe^{i\omega t} \quad (1)$$

Where M , K and H are mass, stiffness and damping matrices and x and f are vectors of response and force. ω is the forcing frequency and t is time.

Assuming a solution of the form $x(t) = xe^{i\omega t}$ and removing time dependence then 1 becomes

$$(-\omega^2 M + (K + iH))x = f \quad (2)$$

Let $x = x_R + ix_I$ then

$$\left. \begin{aligned} (K - \omega^2 M)x_R - Hx_I &= f \\ Hx_R + (K - \omega^2 M)x_I &= 0 \end{aligned} \right\} \quad (3)$$

It is assumed that M , K and H are symmetric and positive definite. We wish to show that for any forcing frequency ω there exists an f , such that all elements of the displacement vector x are mutually in-phase. The analysis is developed for the case where ω is a root of $\det(K - \omega^2 M) = 0$

Then there exists a real non-trivial vector y such that

$$(K - \omega^2 M)y = 0 \quad (4)$$

This suggests a mono-phase solution to 3:

$$\begin{aligned} x_I &= y \\ x_R &= 0 \\ f &= -Hy \end{aligned} \quad (5)$$

Equation 5 shows that when ω is a natural frequency of the undamped system, the displacement vector (which is in quadrature with the excitation) corresponds to the eigenvector of the undamped system. This leads to the following response criterion which is used as a basis for normal mode experiments.

"For a linear system with proportional hysteretic damping, excited by a set of monophasic harmonic forces, a sufficient condition for the response of the system to be in a normal mode is that the displacement vector be in quadrature with the excitation."

This will be noted as a special case of de Veubeke's Characteristic Phase Lag Theory. (Ref.1)

Traill-Nash (Reference 2) has shown that the force distribution required to excite a normal mode may be rationalised by taking into account the number of effective degrees of freedom at any resonant frequency, thus providing a practical basis on which experiments may be designed.

A mathematical justification for using normal modes in forced response analysis is that the H matrix is of a particular form. To make the analysis meaningful and to allow the use of experimental technique we shall introduce the concept of modal damping. We shall attempt to justify the use of modal damping by comparing experiment and theory.

The Use of Uncoupled Modes of Vibration in the Mathematical Model

The displacement vector x may be transformed to principle co-ordinates by the equation

$$x = Yp \quad (6)$$

where Y is the matrix of mode-shapes and p is a vector of principle co-ordinates.

Substituting 6 into 2 and pre-multiplying by Y^T gives.

$$(-\omega^2 M^* + (K^* + iH^*))p = Y^T f \quad (7)$$

where M^* , K^* and H^* are the diagonal matrices of generalised normal mode properties, the diagonal elements of which are :-

$$\begin{aligned} m_j &= y_j^T M y_j, \text{ Generalised Mass of the } j\text{th mode} \\ k_j &= y_j^T K y_j, \text{ Generalised Stiffness of the } j\text{th mode} \\ h_j &= y_j^T H y_j, \text{ Generalised Damping of the } j\text{th mode} \end{aligned} \quad (8)$$

Note that the orthogonality relationships hold :-

$$\begin{aligned} y_i^T M y_j &= 0 \quad i \neq j \\ y_i^T K y_j &= 0 \quad i \neq j \end{aligned} \quad (9)$$

and we assume

$$y_i^T H y_j = 0 \quad i \neq j$$

Taking the j th equation of 7

$$(-\omega^2 m_j + (k_j + ih_j))p_j = y_j^T f \quad (10)$$

$$\text{Let } p_j = a_j e^{ia_j} \quad (11)$$

Substituting 11 into 10 and taking real and imaginary parts

$$\left. \begin{aligned} (k_j - \omega^2 m_j) a_j \cos \alpha_j - h_j a_j \sin \alpha_j &= \mathbf{y}_j^T \mathbf{f} \\ h_j a_j \cos \alpha_j + (k_j - \omega^2 m_j) a_j \sin \alpha_j &= 0 \end{aligned} \right\} \quad (12)$$

Solving 12 for a_j and $\tan \alpha_j$

$$\left. \begin{aligned} a_j &= \mathbf{y}_j^T \mathbf{f} / ((k_j - \omega^2 m_j)^2 + h_j^2)^{1/2} \\ \tan \alpha_j &= h_j / (k_j - \omega^2 m_j) \end{aligned} \right\} \quad (13)$$

If the damping is light then

$$\omega_j = (k_j / m_j)^{1/2} \quad (14)$$

and we introduce the modal loss factor η_j defined by

$$\eta_j = h_j / k_j \quad (15)$$

and let

$$r_j = \omega / \omega_j \quad (16)$$

Substituting 14, 15 and 16 into 13

$$\left. \begin{aligned} a_j &= \mathbf{y}_j^T \mathbf{f} / k_j (1 - r_j^2)^2 + \eta_j^2)^{1/2} \\ \tan \alpha_j &= \eta_j / (1 - r_j^2) \end{aligned} \right\} \quad (17)$$

Note that the rigid-body modes should be included in the calculation of forced response and that for these modes $k_j = h_j = 0$

So we calculate a_j and $\tan \alpha_j$ for rigid-body modes from 13 and for flexural modes from 17. The forced response \mathbf{x} is then calculated by substitution into 6.

The equations 13 and 17 could also be used to calculate forced response from the experimentally derived modal data. However, errors caused by using measured values of damping and static properties can be eliminated by using the measured resonant amplitudes and force sets required to isolate the modes.

If we assume that \mathbf{y}_j in the preceding equations is the measured resonant displacement vector and let \mathbf{f}_j be the force set used to isolate the j th mode, then substituting $r_j = 1$ and $\mathbf{f} = \mathbf{f}_j$ in 17, we have

$$\left. \begin{aligned} a_j &= \mathbf{y}_j^T \mathbf{f}_j / k_j \eta_j \\ \tan \alpha_j &= \infty \end{aligned} \right\} \quad (18)$$

But by definition a_j will be unity in these circumstances so

$$\left. \begin{aligned} 1 &= \mathbf{y}_j^T \mathbf{f}_j / k_j \eta_j \\ \alpha_j &= \pi/2 \end{aligned} \right\} \quad (19)$$

Note that this equation implies that at resonance the structure behaves as a single degree of freedom oscillator.

Dividing the first equation of 17 by $\mathbf{y}_j^T \mathbf{f}_j / k_j \eta_j$

$$\left. \begin{aligned} a_j &= \mathbf{y}_j^T \mathbf{f} \eta_j / \mathbf{y}_j^T \mathbf{f}_j (1 - r_j^2)^2 + \eta_j^2)^{1/2} \\ \tan \alpha_j &= \eta_j / (1 - r_j^2) \end{aligned} \right\} \quad (20)$$

The first equation of 20 is important to the experimenter because at resonance the equation is independent of damping. Thus in situations where it may be considered that only one mode is effective, forced response may be computed for any arbitrary excitation without recourse to measured values of damping or static properties. In the experiments reported herein, equation 20 is used to calculate the forced response to rotor head excitation and the results compared with response measured during actual rotor head excitation.

At resonance the calculated response is dependent only on the measured modal eigenvectors and the measured applied forces, thus minimising the effects of experimental errors.

3. Description of Experiments

Airframe State

The airframe was suspended clear of the ground via heavy duty braided rubber cord. The airframe was ballasted to give a nose-down attitude of 2° , with lumped masses replacing rotors, crew and standard equipment. The attitude was chosen to eliminate free-play between the main rotor shaft and gearbox. The fuel tanks were empty and the transmission system free to rotate. The oleos were completely decompressed.

Figure 1 is a diagram of the experimental set-up.

Isolating and Measuring the Normal Modes

Prior to setting the normal modes some overall "feel" for the dynamic characteristics of the helicopter was achieved by recording the complex frequency response (using single-point excitation) of the structure at a number of points, for a number of exciter positions, to produce a "panorama" of sensitive frequencies and areas of maximum response.

In setting up the normal modes a philosophy of "minimum complexity" was employed, consistent with acceptable results. Where multi-point excitation was required a six-channel MAMA (reference 3) system was employed, thus reducing the work load to a minimum.

The acceptability or otherwise of each mode was based upon the characteristic phase lag criterion, with, in general, an allowable experimental phase error of $\pm 10^{\circ}$ of total in-phase velocity response at all points on the structure.

For each of the five modes investigated the modal properties were recorded in terms of shape, natural frequency, complex frequency response, orthogonality (with respect to the mass matrix) and modal damping. Evidence of modal non-linearity was also recorded.

Each mode shape was recorded at 95 points. With vertical, lateral and fore-and-aft measurements at each point this resulted in a response vector of order 285.

Response was measured using the integrated signal from a piezoelectric accelerometer/charge amplifier system. The resultant voltage, which was essentially in-phase with the applied force-set (itself monitored using vibrator currents) was fed from the MAMA Transfer Function Analyser to a semi-automatic data-reduction facility which recorded, for each point, the three vibration amplitudes onto punched card.

Complex plotting of amplitude vs frequency was done via the Transfer Function Analyser and X-Y plotter. Modal damping was assessed using the 'half power' technique and by using the relationship between dynamic magnifier 'Q' and rate-of-change of phase with respect to frequency around each natural frequency.

Forced response experiments were performed by representing rotor loads with a large electromagnetic vibrator producing uniaxial in-plane force at the rotor head.

Figure 2 identifies the main elements of the experimental equipment.

4. Creation of the Mathematical Model

The data obtained from earlier experimental stiffness tests on the Wessex was initially rationalised by assuming that the fuselage could be represented by beams with linear taper in EI and GJ. Such beam elements are very attractive for a coarse finite element model since they enable a complicated stiffness and mass distribution to be represented with many fewer degrees of freedom than would be required if uniform elements were used.

Geometry

Figure 3 shows the geometry of the model of the Wessex, the numbers referring to the joints of the beams.

The positions of nodes 1, 2, 3, 4, 5, 6, 7, 10, 15, 18 and 19 were dictated solely by geometric considerations. Nodes 8, 9, 11 and 13 were added to enable the stiffness distributions to be accurately represented and it was thought that these 15 nodes enabled the mass distribution to be adequately represented too.

It was found, however, that nodes 12, 14, 16 and 17 were required in the less-stiff rear end of the fuselage and tail pylon to provide sufficient degrees of freedom to adequately represent the shapes of the higher frequency normal modes. There are 6 degrees of freedom at each mode, 3 translations and 3 rotations.

Stiffness

Each element of the model is capable of deforming axially, torsionally, in bending and in transverse shear, so its stiffness characteristics are defined by EA, GJ, EI in two perpendicular axes and GA.

The engines, gearbox components, rotor head mass and tail rotor mass were free to rotate but interconnected by shafts but as the inertia of this system was unlikely to be overcome the main rotor and tail rotor masses were assumed to be rigidly attached to the main rotor pylon and tail rotor support arm respectively.

Mass

The mass distribution of the Wessex was refined by breaking down the major non-structural items together with all structural components into many small masses, whilst maintaining the centre of gravity positions of each item and the moments of inertia of the whole aircraft.

It was found that a very fine breakdown was required at the more flexible tail end of the airframe to correctly represent the kinetic energy of the structure in the higher frequency normal modes.

Lumped-mass models proved to be very poor when the normal modes were compared with the experimentally derived normal modes, with only the first mode being of satisfactory accuracy. This was due to the inability of a lumped mass system, in a very coarse model, to correctly represent the kinetic energy of sections of structure which have significant motion in translational and rotational directions simultaneously in the normal modes.

The formulation of the consistent mass matrices enabled non-structural point masses to be attached anywhere on the elements.

5. Discussion of Results

Relevance of the Theory in the Light of Experimental Evidence

The initial assumptions on which the normal-mode theory is based are that the structure is linear and that the dissipative characteristics may be described by proportional hysteretic damping.

Proportional hysteretic damping was assumed because such an assumption has been justified on similar complicated structures. The 'Wessex' experiments have tended to confirm the general concept of modal damping although it has been found that the modal dampings, whilst generally increasing with frequency, do not follow any simple pattern.

One task of the research was to assess the use of multi-point excitation on helicopter structures. It has been found that the rationalisation of the number of exciters used, due to Traill-Nash, was justified, but one point particularly relevant to helicopters was that exciters should be used (even if at very low force) at the rotor head to ensure that the components of the eigenvectors representing head motion are fully excited. In this way any backlash or local non-linearities are taken into account. It was found that no more than 3 exciters were required to achieve total in-phase velocity response to within $\pm 10^\circ$ (a reasonable practical limitation) in any mode.

It was found that the generalised mass matrix (Fig. 4) compares favourably with the theoretical ideal (equations 8 and 9), i.e. the off-diagonal terms were small compared to the diagonals. It was found however that the generalised mass matrix, whilst giving confidence in the experimental measurements, could not be relied upon to give an assessment of the value of the measured modes in the forced-response case.

It was found that on the whole, the modal frequency dependences (figures 5, 8, 11, 14 and 16) show fair agreement with the single-degree-of freedom concept. In the 9.48 Hz mode no explanation can be given for the bump at the high frequency end of the complex plot. No explanation can be given for the sudden decrease in the modulus of the response around the resonant frequency of the response around the resonant frequency of the 20.1 Hz mode.

In measuring modal damping, it was found the relationship between $d\phi/d\omega$ and ' Q ' was more accurate than the half-power technique.

Superposition of the normal modes and comparison with experimental forced response provides the key to validating the normal-mode approach to forced response. The peak amplitudes are independent of measured damping values and static stiffness properties and hence discrepancies would indicate errors in the measurement of resonant amplitudes, errors in force measurement or invalidity of the theory.

Errors in the damping would be manifested by divergence of the slopes either side of the peaks from the slopes of the forced response. Figure 19 (which is typical of a large number of points) indicates that there is fair agreement between the super-position of normal modes and forced response.

Comparison of Theoretically and Experimentally Derived Normal Modes

Figures 6 and 7 show the mode shapes of the first mode of the airframe and model respectively. The frequency error for this mode is 1.4% and the deflections at the head are accurate to within 3%. These errors cause an error of about 15% in the modulus of the response of the mode to a 15 Hz excitation

force at the main rotor head (a_j in equation 17). Note that the experimentally derived values of modal damping are used when superimposing both sets of modes so the error in phase of response to a 15 Hz excitation is due solely to the error in the frequency.

Figures 9 and 10 show the second modes of airframe and model. The frequency is accurate to .3%.

Figures 12 and 13 show the third mode of airframe and model. The frequency is accurate to .3% but the mode shape appears at first glance to be rather inaccurate. The two shapes are normalised to give the same maximum deflection but the position of the maximum differs. However the shapes of the fuselage deflections are very similar apart from the scale, which suggests that the main undercarriage is poorly represented in the model. There was found to be a lot of 'play' in the bearings of the main undercarriage legs and no attempt was made to incorporate this in the model. The deflection at the rotor head is very accurate so the modulus of the response to 15 Hz rotor head excitation is also accurate.

Figures 15 and 16 show the fourth modes of airframe and model. The frequency is not very accurate (2.3% error) but this only causes an error of 2 degrees in the phase of the response of the mode to 15 Hz excitation and this is acceptable. The general shape of the mode is recognisable as being the same mode but it differs in details. There are differences in the deflection of the main rotor head which affects the prediction of response to excitation forces applied at the rotor head. There is also some frame deformation in the airframe mode which the model is incapable of representing.

Figure 18 shows the fifth mode of the airframe. There are gross deformations of the frames so there is no comparable mode of the model. The model predicts the first three normal modes sufficiently accurately. The prediction of the fourth mode could be greatly improved by modelling the main rotor pylon in much greater detail. The fifth and higher modes would involve a model with many more degrees of freedom.

6. Conclusions

The experiments and theoretical analysis on a Wessex helicopter confirm, in general, the validity of the normal mode approach to the helicopter forced response problem.

It was found that the equipment and techniques, specifically adapted for helicopter shake-testing, were well suited for the task in hand. It was found that de Veubeke's Characteristic Phase Lag Criterion, modified to allow phase errors of up to -10° at areas of significant response, produced results that were broadly confirmed by forced response analysis. It was found that a maximum of three exciters were required to achieve the necessary modal purity in all five normal modes measured in the frequency range up to 21 Hz.

The derivation of modal damping from the $d\phi/d\omega/Q$ relationship was found to be more reliable than the half-power method. The damping values obtained, however, are still not considered to be particularly accurate.

The theoretical analysis, based upon a dynamic model with 114 degrees of freedom, demonstrated that coarse branched beam analysis adequately represented the first three normal modes. The representation of higher modes would require an increase in model complexity.

It was found that in dynamic analysis using coarse idealisation, the use of a consistent mass matrix was required to achieve the necessary accuracy of

the modes.

It was found that the generalised mass matrix, whilst representing a satisfactory degree of orthogonality (i.e. small off-diagonal terms) was inadequate in confirming the usefulness of the normal modes in the forced response case.

The use of the 'total dynamics' concept where one small multi-disciplinary team is responsible for the entire project, from inception to final report stage, was totally justified.

Acknowledgements

The author acknowledges the essential contributions made by R.J.Parker, T. Yarker and R.L. Mattravers of the Research Department of Westland Helicopters Limited both in the execution of the research and in the preparation of the paper.

This work has been carried out with the support of the Procurement Executive, Ministry of Defence.

References

1. A variational Approach to Pure Mode Excitation Based upon Characteristic Phase Lag Theory.
B.M. Fraejijs de Veubeke
AGARD Report 39 April 1956
2. On the Excitation of Pure Natural Modes in Aircraft Resonance Testing.
R. W. Traill-Nash
A.R.L. Report SM 254 July 1957
3. MAMA - A Semi-Automatic Technique for Exciting the Principle Modes of Vibration of Complex Structures
G.A. Taylor
D.R. Gaukroger
C.W. Skingle
H.M.S.O. RM No. 3590, 1969

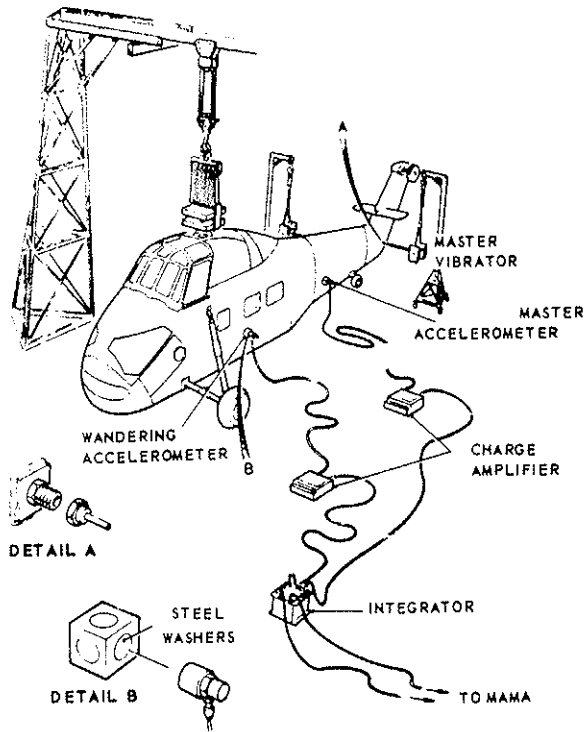


FIG.1. GENERAL ARRANGEMENT

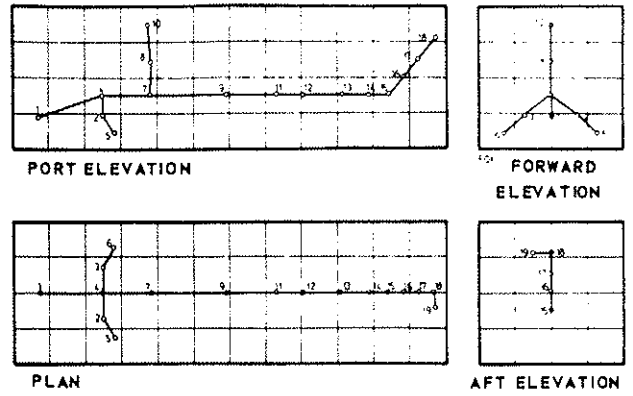


FIG.3. GEOMETRY OF MATHEMATICAL MODEL

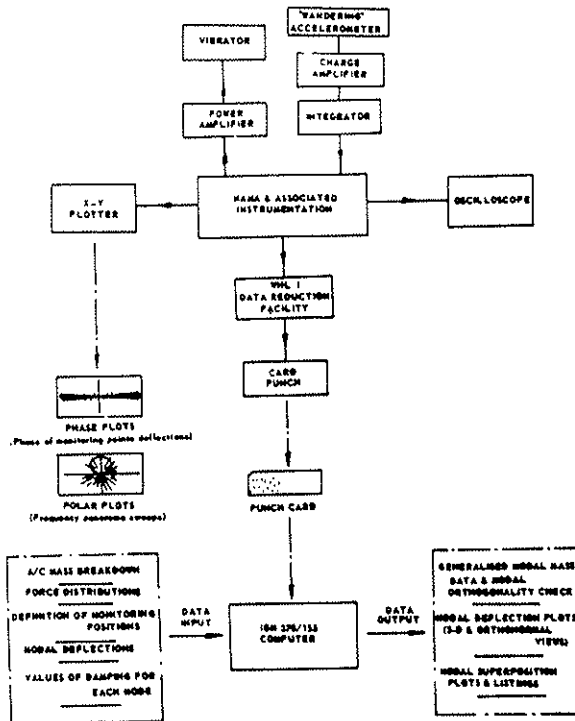


FIG.2. DATA ACQUISITION

	5.72	9.52	13.55	16.88	20.79	Hz
5.72	1	0.084	-0.012	-0.049	0.036	
9.52	0.084	1	0.024	-0.202	-0.040	
13.55	-0.012	0.024	1	-0.094	-0.068	
16.88	-0.049	-0.202	-0.094	1	0.002	
20.79	0.036	-0.040	-0.068	0.002	1	
Hz						

FIG.4. EXPERIMENTAL GENERALISED MASS MATRIX

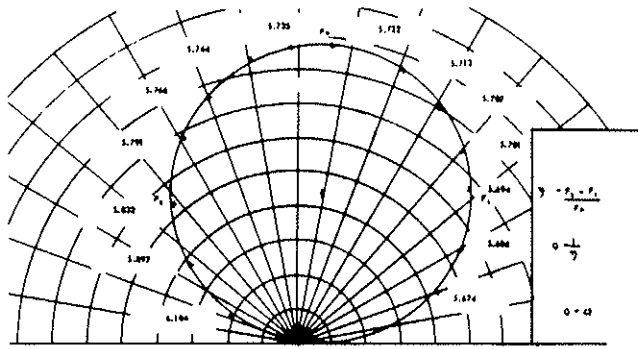


FIG. 5. 5.73 Hz MODE.
COMPLEX FREQUENCY RESPONSE

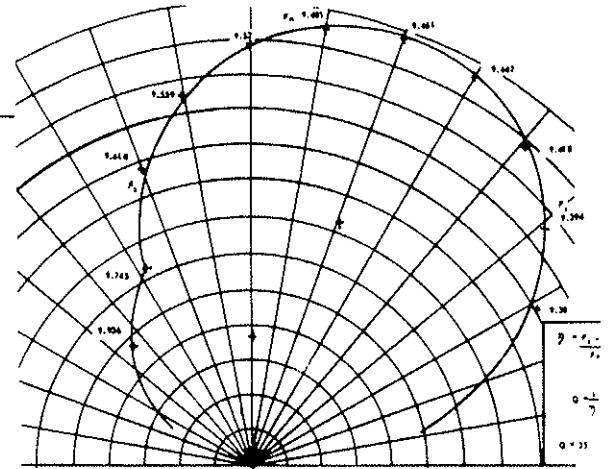


FIG. 8. 9.48 Hz MODE.
COMPLEX FREQUENCY RESPONSE

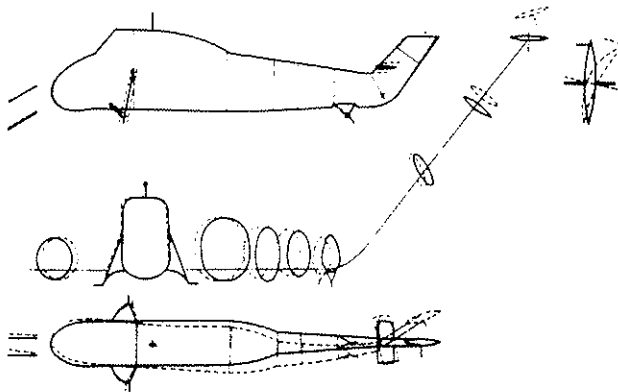


FIG. 6. 5.73 Hz MODE.
EXPERIMENTAL MODE SHAPE

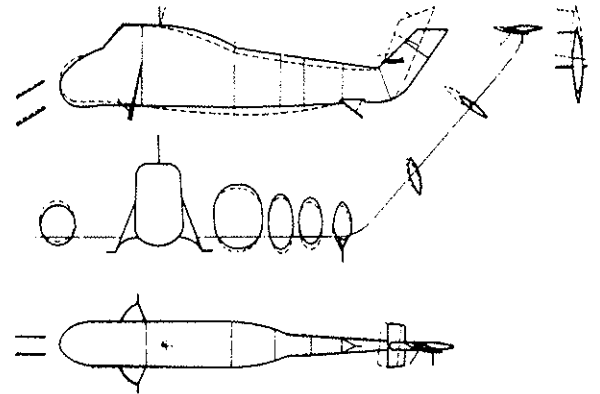


FIG. 9. 9.48 Hz MODE.
EXPERIMENTAL MODE SHAPE

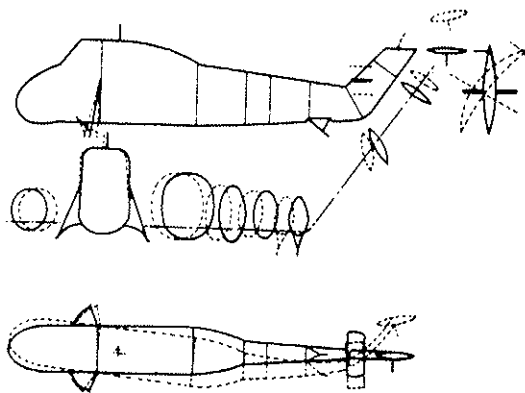


FIG. 7. 5.73 Hz MODE.
THEORETICAL MODE SHAPE

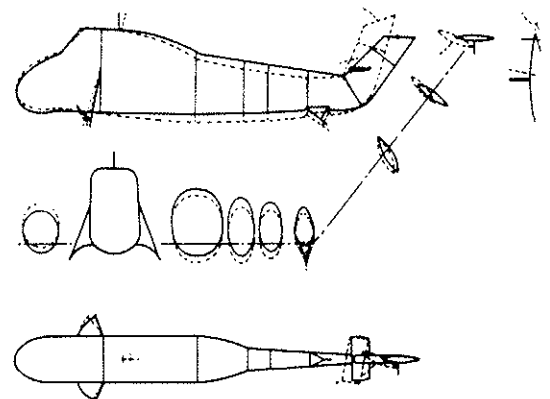


FIG. 10. 9.48 Hz MODE.
THEORETICAL MODE SHAPE

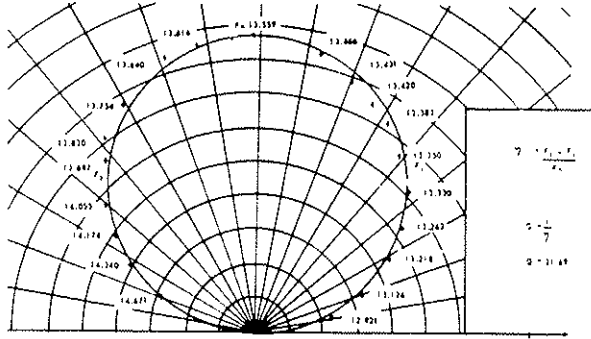


FIG. 11. 13.56 Hz MODE
COMPLEX FREQUENCY RESPONSE

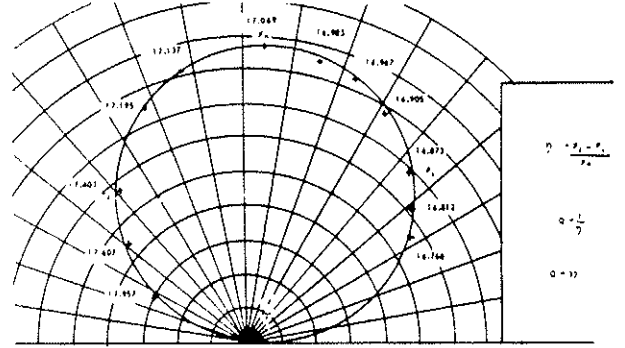


FIG. 14. 17.06 Hz MODE
COMPLEX FREQUENCY RESPONSE

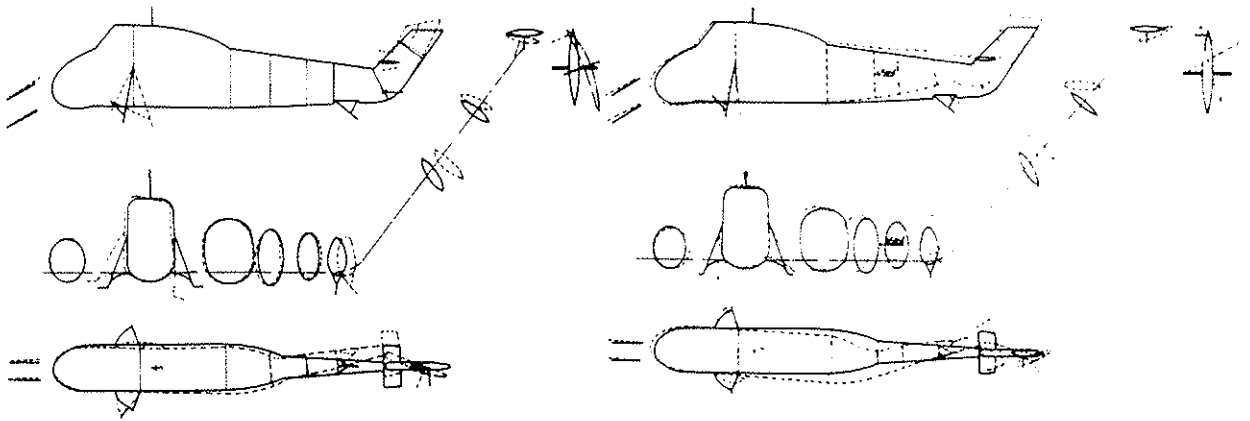


FIG. 12. 13.56 Hz MODE.
EXPERIMENTAL MODE SHAPE

FIG. 15. 17.06 Hz MODE.
EXPERIMENTAL MODE SHAPE

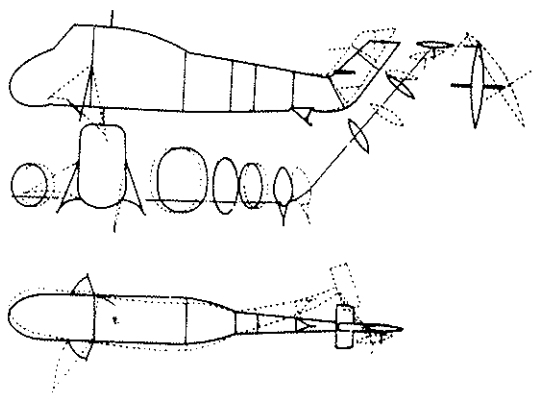


FIG. 13. 13.56 Hz MODE.
THEORETICAL MODE SHAPE

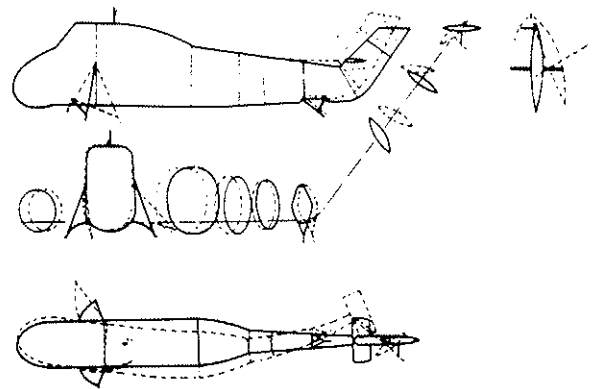


FIG. 16. 17.06 Hz MODE.
THEORETICAL MODE SHAPE

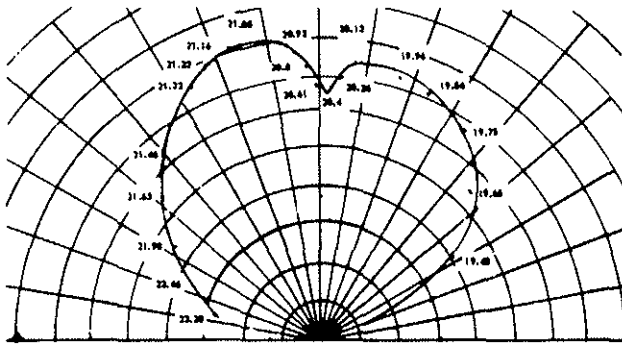


FIG. 17. 20.1 Hz MODE.
COMPLEX FREQUENCY RESPONSE

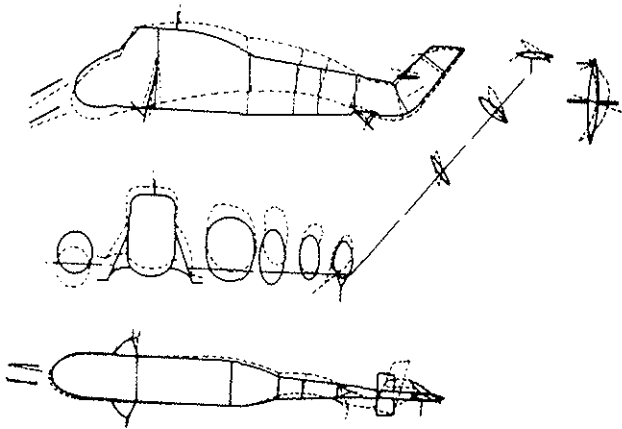


FIG. 18. 20.1 Hz MODE.
EXPERIMENTAL MODE SHAPE

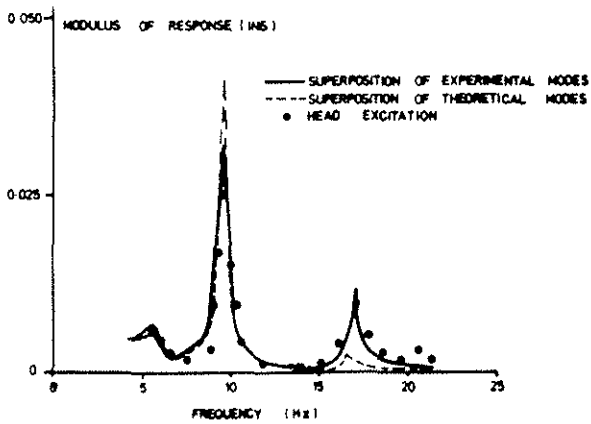


FIG. 19. FORCED RESPONSE ANALYSIS.
100 LB FORE-AND-AFT EXCITATION
AT MAIN ROTOR. FORE-AND-AFT
RESPONSE AT PILOT